Numerical investigation of the transient cavitating flow and vortical patterns around a hydrofoil

Q Wu[1], M J Zhang[2], B Huang[2], G Y Wang[2] and S L Cao[1]

1 Department of Thermal Engineering, Tsinghua University, Beijing 100081, China
2 School of Mechanical Engineering, Beijing Institute of Technology, Beijing, China

Email: wuqin919@163.com

Abstract. The objective of this work is to investigate the cavitating flow mechanism of a specific hydrofoil, Tulin hydrofoil, and better understand the vortex-cavitation interactions in transient cavitating flows. The numerical investigations are performed using a large eddy simulation method and the Zwart cavitation model. The predicted cavity formation and evolution agree well with the experimental observation. An asymmetric vortex street has been formed, with the upper one (the trailing edge vortex street) has a regular vortex shape and a clear boundary between vortex structures, while the lower one (the leading edge vortex street) has a larger cavitation area due to the low pressure distribution on the suction side of the foil. The turbulent kinetic energy transport equation has been adopted to examine the balance and contribution of different mechanisms. The formation and evolution of the leading and trailing edge vortex structures are responsible for the generation and modification of the turbulent kinetic energy distributions. The convection term varies significantly in the cavity region during the phase change process, and the boundary of the vortex structures enhance the production term of the turbulent kinetic energy.

1. Introduction

Cavitation generally occurs when the local fluid pressure reduces to the saturated vapor pressure and consequently the gas filled or gas and vapor filled bubbles are formed. Owing to its great importance in a wide range of applications, much effort has been made to study the fundamental physics of the cavitating flow[1-4]. With the decreasing of the cavitation number in a specific flow condition, the cavitating flow displays several patterns: incipient cavitation, sheet cavitation, cloud cavitation and supercavitation[5-8]. With the development of the experimental and numerical technique, more attention has been paid to the complex interaction between phase-change and vortex structures in cavitating flow. Kawanami et al.[9] investigated the cloud cavitation through a series of experiments and presented the close relationship between the formation of cloud cavity and the re-entrant jet. Ausoni et al.[10] conducted the experimental studies to investigate the effects of cavitation on vortex generation mechanism. They found that the vortex-induced vibration level significantly increased at cavitation onset and the transverse velocity at the hydrofoil trailing edge increased the vortex strength. Due to the improvement of computing technique, numerical simulations have played an important role in capturing the interaction between the cavitation patterns and turbulent flow structures. Huang et al.[11] investigated the sheet/cloud cavitating flow turbulent structures and provided the interaction between the unsteady cavitating flow and vortex dynamics. The results showed strong correlation between the cavities and vortex structures and the cavitation development significantly change the interaction between leading and trailing edge vortices. Ji et al. [12] numerically investigated the structure of

cavitating flow around a twisted hydrofoil and revealed that cavitation promotes vortex production and increases the flow unsteadiness.

The objective of this paper is to numerically investigate the cavitating flow around the Tulin hydrofoil, which has a sharp leading edge and a relatively thick trailing edge, with focus on the intrinsic relationships between the cavity patterns and the vortex structures.

2. Numerical model

2.1. Governing equations

The numerical simulations are performed by solving the incompressible and unsteady Reynolds Average Navier-Stokes (URANS) equations via the commercial CFD software ANSYS CFX.

$$\frac{\partial \rho_m}{\partial t} + \frac{\partial (\rho_m u_j)}{\partial x_j} = 0, \tag{1}$$

$$\frac{\partial (\rho_m u_i)}{\partial t} + \frac{\partial (\rho_m u_i u_j)}{\partial x_j} = -\frac{\partial p}{\partial x_i} + \frac{\partial}{\partial x_j}(\mu_m \frac{\partial u_i}{\partial x_j}), \tag{2}$$

$$\frac{\partial \rho_l \alpha_l}{\partial t} + \frac{\partial (\rho_l \alpha_l u_j)}{\partial x_j} = \dot{m}^+ + \dot{m}^-, \tag{3}$$

$$\rho_m = \rho_l \alpha_l + \rho_v \alpha_v, \tag{4}$$

$$\mu_m = \mu_l \alpha_l + \mu_v \alpha_v. \tag{5}$$

where u is the velocity, p is the pressure, ρ_m is the mixture density, ρ_l is the liquid density, ρ_v is the vapor density, μ_m is the mixture viscosity, μ_l and μ_v are respectively the liquid and vapor dynamic viscosity. α_v is the vapor fraction, α_l is the liquid fraction. The subscripts (i, j, k) denote the directions of the Cartesian coordinates. The source term $\dot{m}^+$, and the sink term $\dot{m}^-$, in equation (3) represent the condensation and evaporation rates, respectively.

Large Eddy Simulation (LES) is about filtering of the equations of movement and decomposition of the flow variables into a large scale (resolved) and a small scale (unresolved) parts. By performing the volume averaging and neglecting density fluctuations, the filter Navier-Stokes equations become:

$$\frac{\partial (\rho_m \overline{u}_i)}{\partial t} + \frac{\partial (\rho_m \overline{u}_i \overline{u}_j)}{\partial x_j} = -\frac{\partial \overline{p}}{\partial x_i} + \frac{\partial}{\partial x_j}(\mu_m \frac{\partial \overline{u}_i}{\partial x_j}) - \frac{\partial (\rho_m \tau_{ij})}{\partial x_j}, \tag{6}$$

τ_{ij} is the sub-grid scale (SGS) stress, which is defined as:

$$\tau_{ij} = \overline{u_i u_j} - \overline{u}_i \overline{u}_j \tag{7}$$

In present simulation, the Smagorinsky model[13] is used, where the sub-grid scale (SGS) stress is assumed to be proportional to the modulus of the strain rate tensor S_{ij} of the filtered large-scale flow:

$$\tau_{ij} = -2 \bullet \nu_{SGS} \bullet \overline{S}_{ij} = \nu_{SGS} \bullet \left(\frac{\partial \overline{u}_i}{\partial x_j} + \frac{\partial \overline{u}_j}{\partial x_i} \right) \tag{8}$$

The SGS viscosity ν_{SGS} are modeled by:

$$\nu_{SGS} = (C_S \Delta)^2 \left| \overline{S} \right| \tag{9}$$

$$\left| \overline{S} \right| = (2 \overline{S}_{ij} \overline{S}_{ij})^{1/2} \tag{10}$$

with the Smagorinsky constant C_S =0.18, which is the default values in CFX, Δ is the local grid size, namely,

$$\Delta_{grid,2D} = (\Delta x \bullet \Delta y)^{1/2} \text{ and } \Delta_{grid,3D} = (\Delta x \bullet \Delta y \bullet \Delta z)^{1/3} \quad (11)$$

where Δx, Δy and Δz are the mesh sizes in each direction.

2.2. Cavitating model

The Zwart cavitation model[14] are introduced to the cavitating flow simulations, with the source and sink terms defined as:

$$\dot{m}^- = -C_{dest}\frac{3\alpha_{nuc}(1-\alpha_v)\rho_v}{R_B}\left(\frac{2}{3}\frac{p_v - p}{\rho_l}\right)^{1/2}, p < p_v \quad (12)$$

$$\dot{m}^+ = C_{prod}\frac{3\alpha_v\rho_v}{R_B}\left(\frac{2}{3}\frac{p - p_v}{\rho_l}\right)^{1/2}, p > p_v \quad (13)$$

where α_{nuc} is the nucleation volume fraction, R_B is the bubble diameter, p_v is the saturated liquid vapor pressure, and p is the local fluid pressure. C_{dest} is the rate constant for vapor generated from the liquid in a region where the local pressure is less than the vapor pressure. Conversely, C_{prod} is the rate constant for re-conversion of vapor back into liquid in regions where the local pressure exceeds the vapor pressure. In this work, the assumed model constants are $\alpha_{nuc}=5\times10^{-4}$, $R_B=1\times10^{-6}$m, $C_{dest}=50$, and $C_{prod}=0.01$, which are the default values in CFX, and are used because of their supposed general applicability.

2.3. Numerical setup

The computational domain and boundary conditions are given according to the experimental setup[15], which is shown in Figure 1. The hydrofoil is subjected to a nominal free stream velocity of $U_\infty=10$m/s, yielding a moderate Reynolds number of $Re=U_\infty c/\nu=7.0\times10^5$, where c is the chord length and ν is the dynamic viscosity of the liquid (water at 25°C). The outlet pressure is set according to the cavitation number $\sigma=(p_\infty-p_v)/(0.5\rho_l U_\infty^2)=1.27$, where p_∞ is the tunnel pressure, p_v is the saturated vapor pressure. The angle of attack of the hydrofoil is set to be $\alpha=15°$ for the simulations.

Figure 2 shows the 2D fluid mesh, which is refined near the leading and trailing edge of the foil and in the wake region to satisfy $y^+=yu_\tau/\nu\approx1$, where y is the distance from the first cell to the foil surface, u_τ is the wall frictional velocity. The total mesh nodes number is 503,140 nodes.

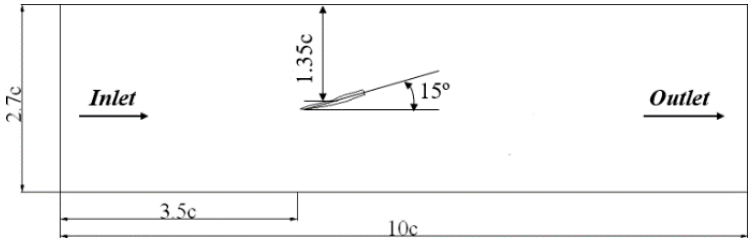

Figure 1. Computational domain and boundary conditions

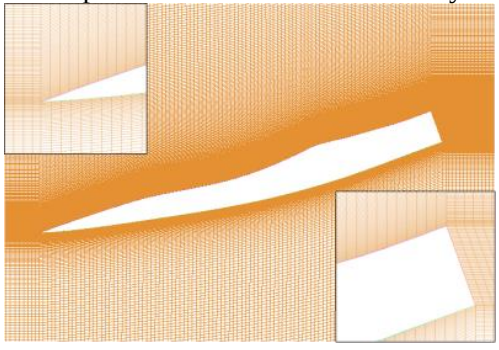

Figure 2. Mesh distributions

3. Results and discussions

Figure 3 shows the time evolution of the cavity and the vortical patterns. Good agreement can be obtained between the experimental observation and numerical simulations, the cavity forms and sheds at the leading and trailing edge of the foil alternatively. From both the vapor and vorticity contours, it can be observed that the cavities always concentrate in the center area of the vortex structures. At $t=t_1$, the cavity at the leading edge of the foil has already formed and instead of the cavity attachment and development in length, the cavity rolls into a small-scale cloud cluster, corresponding to the counter-clockwise vortex structures. Meanwhile, another cluster of cavity, as well as a clockwise vortex, begin to form at the trailing edge of the foil, as shown in figure 3(a). From t_2 to t_3, the leading edge vortex structure shed downstream, along with the development of the cavity cluster. And the trailing edge vortex structure further develops, with clear vortex boundary being observed, as shown in figures 3(b) and (c). Until $t=t_4$, the leading edge vortex has moved downstream to the trailing edge of the foil, the counter-rotating vortex structures interact with each other, so that both vortex structures shed from the foil, accompanied with the cavity collapse, as shown in figures 3(d) and (e). With the time increasing, a asymmetric vortex street has been well formed, as shown in figure 4. The upper one (the trailing edge vortex street) has a more regular vortex shape and more clear boundary between vortex structures, while the lower one (the leading edge vortex street) has a larger cavitation area due to the low pressure distribution on the suction side of the foil.

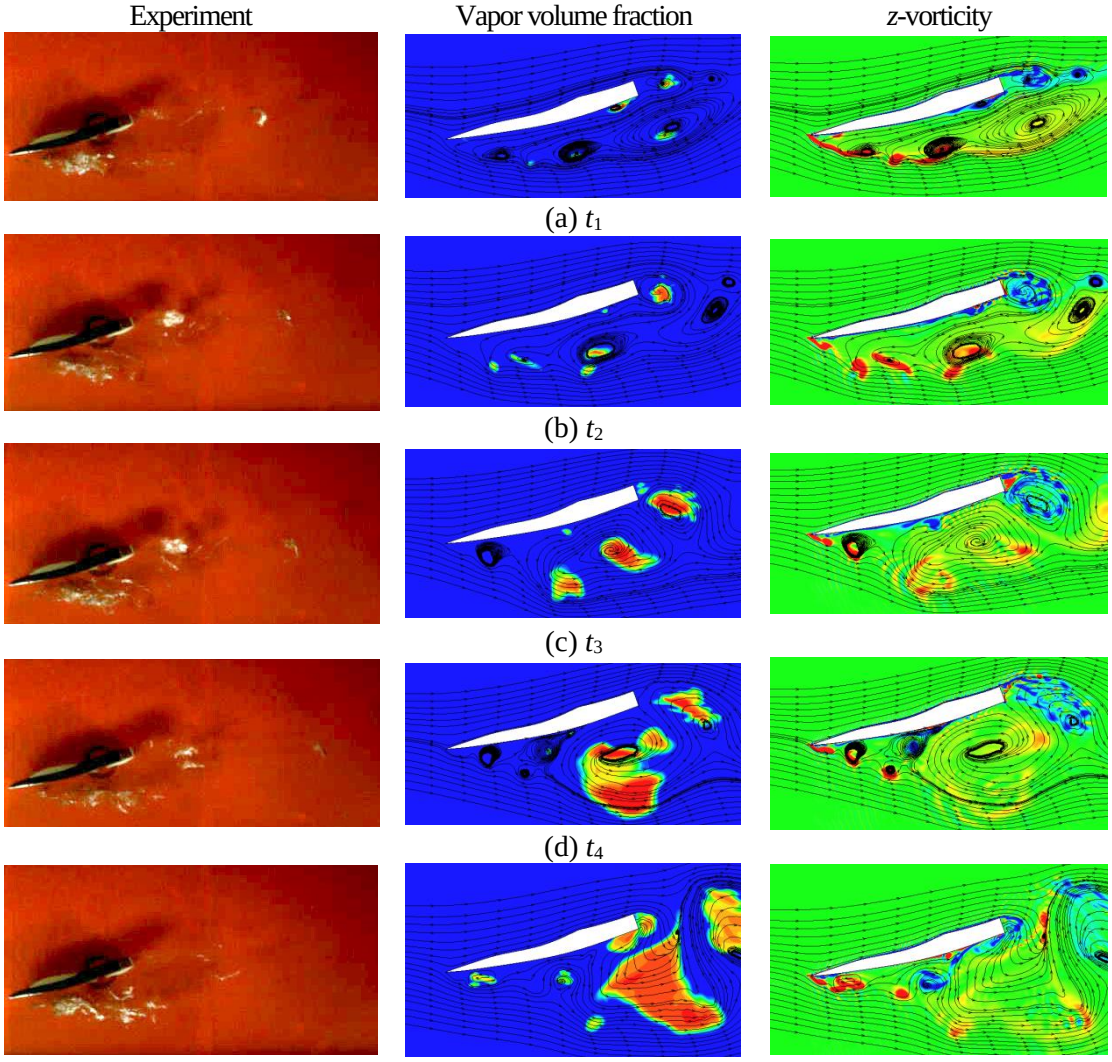

(e) t_5

Figure 3. Evolution of the cavity patterns and vortex structures

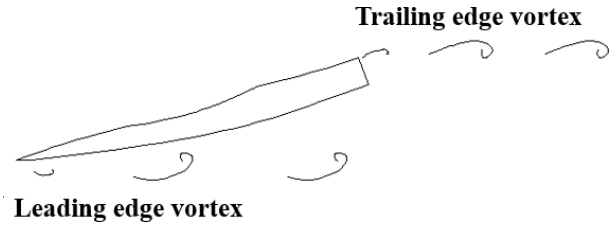

Figure 4. Illustration of the leading and trailing edge vortex structures

To further investigate the vortex-cavitation interaction and examine the balance and contribution of different mechanisms, the turbulent kinetic energy transport equation has been adopted. A generic form of the turbulent kinetic energy transport equation for incompressible flow[16] is given by:

$$\frac{dk}{dt}=\frac{\partial k}{\partial t}+\langle u_k\rangle\frac{\partial k}{\partial x_k}=-\langle u_i' u_k'\rangle\frac{\partial\langle u_i\rangle}{\partial x_k}-\frac{\partial}{\partial x_k}\left(\frac{\langle p' u_k'\rangle}{\rho}+\left\langle\frac{1}{2}u_i' u_i' u_k'\right\rangle-\nu\frac{\partial k}{\partial x_k}\right)-\nu\left\langle\frac{\partial u_i'}{\partial x_k}\frac{\partial u_i'}{\partial x_k}\right\rangle \quad (14)$$

where k is the turbulent kinetic energy per unit mass, the left side of the equation represents the material derivative of the turbulent kinetic energy and the terms on the right side of the equation are, the convection term, the turbulence production term, the diffusion term and the dissipation term. Figure 5 shows the time evolution of the convection term, the production term, the diffusion term and the dissipation term. As demonstrated in figure 5, the formation and evolution of the leading and trailing edge vortex structures are responsible for the generation and modification of the turbulent kinetic energy distributions. The convection term varies significantly in the cavity region during the phase change process, and the boundary of the vortex structures enhance the production term of the turbulent kinetic energy.

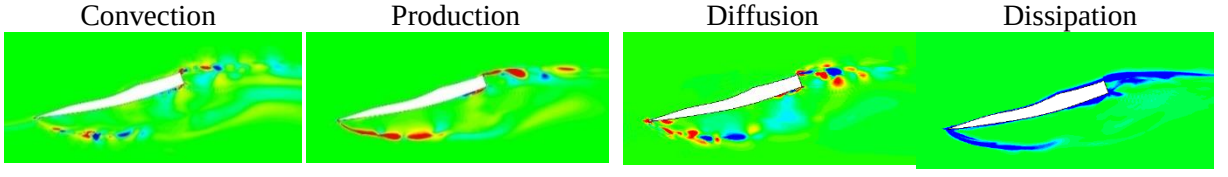

(a) t_1

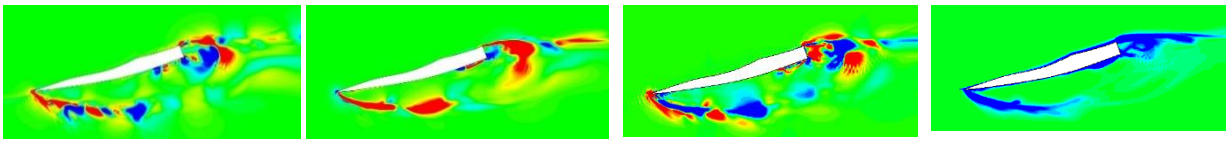

(b) t_2

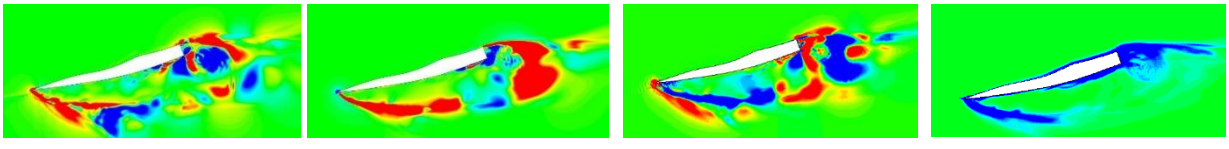

(c) t_3

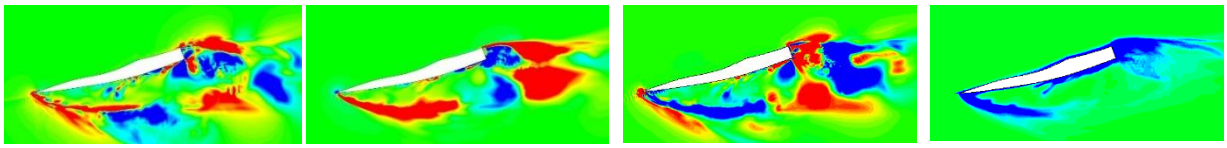

(d) t_4

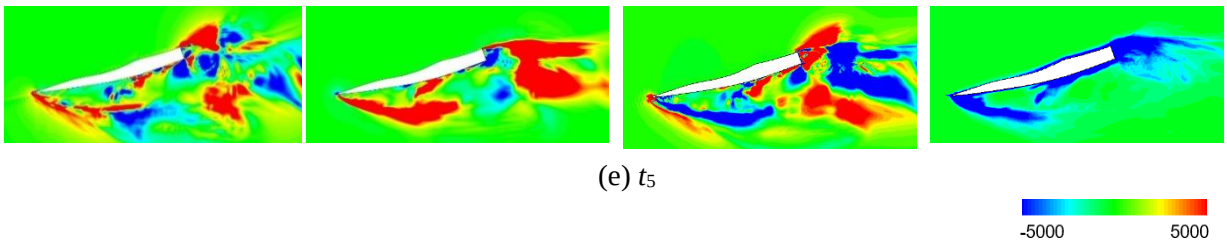

(e) t_5

Figure 5. Turbulent kinetic energy budget for the cavitating flow

4. Conclusions

In this work, the numerical investigations are performed on a Tulin hydrofoil, which has a sharp leading edge and a relatively thick trailing edge, using a large eddy simulation method and the Zwart cavitation model. The main findings are as follows:

Good agreement can be obtained between the experimental observation and numerical simulations and the cavity forms and sheds at the leading and trailing edge of the foil alternatively. Meanwhile, an asymmetric vortex street has been formed, with the upper one (the trailing edge vortex street) has a regular vortex shape and a clear boundary between vortex structures, while the lower one (the leading edge vortex street) having a larger cavitation area due to the low pressure distribution on the suction side of the foil.

From the turbulent kinetic energy transport equation, the formation and evolution of the leading and trailing edge vortex structures are responsible for the generation and modification of the turbulent kinetic energy distributions. The convection term varies significantly in the cavity region during the phase change process, and the boundary of the vortex structures enhance the production term of the turbulent kinetic energy.

Acknowledgement

The authors gratefully acknowledge the support by the National Postdoctoral Program for Innovative Talents (BX201700126), the China Postdoctoral Science Foundation (Grant No: 2017M620043) and the Natural Science Foundation of Beijing Municipality (No. 3172029).

References

[1] Brennen, C.E., 1995. Cavitation and bubble dynamics, Annual Review of Fluid Mechanics.
[2] Wu, Q., Wang, Y., Wang, G., 2017. Experimental investigation of cavitating flow-induced vibration of hydrofoils. Ocean Engineering, 144(1): 50-60.
[3] Joseph, D.D., 1995. Cavitation in a flowing liquid. Phys. Rev. E 51, 1649-1650.
[4] Wu, Q., Huang, B., Wang, G., Gao, Y., 2015. Experimental and numerical investigation of hydroelastic response of a flexible hydrofoil in cavitating flow. International Journal of Multiphase Flow, 74, 19-33.
[5] Wang, G.Y., Senocak, I., Shyy, W., et al., 2001. Dynamics of attached turbulent cavitating flows. Progress in Aerospace Sciences. 37, 551-581.
[6] Foeth, E.J., Van Doorne, C.W.H., Van Terwisga, T., Wieneke, B., 2006. Time resolved PIV and flow visualization of 3D sheet cavitation. Exp. Fluids 40, 503-513.
[7] Coutier-Delgosha, O., Reboud, J.L., Dellanoy, Y., 2003. Numerical simulation of the unsteady behaviour of cavitating flows. Int. J. Numer. Methods Fluids 42, 527-548.
[8] Li, X., Wang, G., Zhang, M., Shyy, W., 2008. Structures of supercavitating multiphase flows. Int. J. Therm. Sci. 47, 1263-1275.
[9] Kawanami, Y., Kato, H., Yamaguchi, H., Tanimura, M., Tagaya, Y., 1997. Mechanism and control of cloud cavitation. ASME Journal of Fluids Engineering. 119(4), 788-794.
[10] Ausoni, P., Farhat, M., Escaler, X., Egusquiza, E., Avellan, F., 2007. Cavitation Influence on von Kármán Vortex Shedding and Induced Hydrofoil Vibrations. J. Fluids Eng. 129, 966-

973.
[11] Huang, B., Zhao, Y., Wang, G., 2014. Large eddy simulation of turbulent vortex-cavitation interactions in transient sheet/cloud cavitating flows. Comput. Fluids 92, 113-124.
[12] Ji, B., Luo, X. W., Wu, Y. L., Peng, X. X., Duan, Y. L., 2013. Numerical analysis of unsteady cavitating turbulent flow and shedding horse-shoe vortex structure around a twisted hydrofoil. International Journal of Multiphase Flow. 51, 33-43.
[13] Smagorinsky J., 1963. General Circulation Experiments with the Primitive Equations 1. The Basic Experiment. Monthly Weather Review, 91(3): 99-164.
[14] Zwart, P., Gerber, A., Belamri, T., 2004. A two-phase flow model for predicting cavitation dynamics. Fifth Int. Conf. Multiph. Flow, Yokohama, Japan.
[15] X. Li, G. Wang, M. Zhang, et al., 2006. High-speed observations of cavitating vortices around a hydronautics foil. Journal of Engineering Thermophysics, 27(3): 426-428.
[16] Hinze, J.O., 1975. Turbulence. McGraw-Hill, New York.